Supporting information for

Discharge voltage profile changes via physicochemical phenomena in cycled all-solid-state cells based on $Li_{10}GeP_2S_{12}$ and $LiNbO_3$-coated $LiCoO_2$

Xueying Sun [a], Yuto Yamada [b], Satoshi Hori [b], Yuxiang Li [a], Kota Suzuki [a], Masaaki Hirayama [a], and Ryoji Kanno *[b]

[a.] *Department of Chemical Science and Engineering, School of Materials and Chemical Technology, Tokyo Institute of Technology, 4259 Nagatsuta, Midori, Yokohama 226-8502, Japan.*

[b.] *Research Center for All-Solid-State Battery, Institute of Innovative Research (IIR), Tokyo Institute of Technology, 4259 Nagatsuta, Midori, Yokohama 226-8502, Japan*

***Corresponding Author:** (R.K.) E-mail: kanno@echem.titech.ac.jp

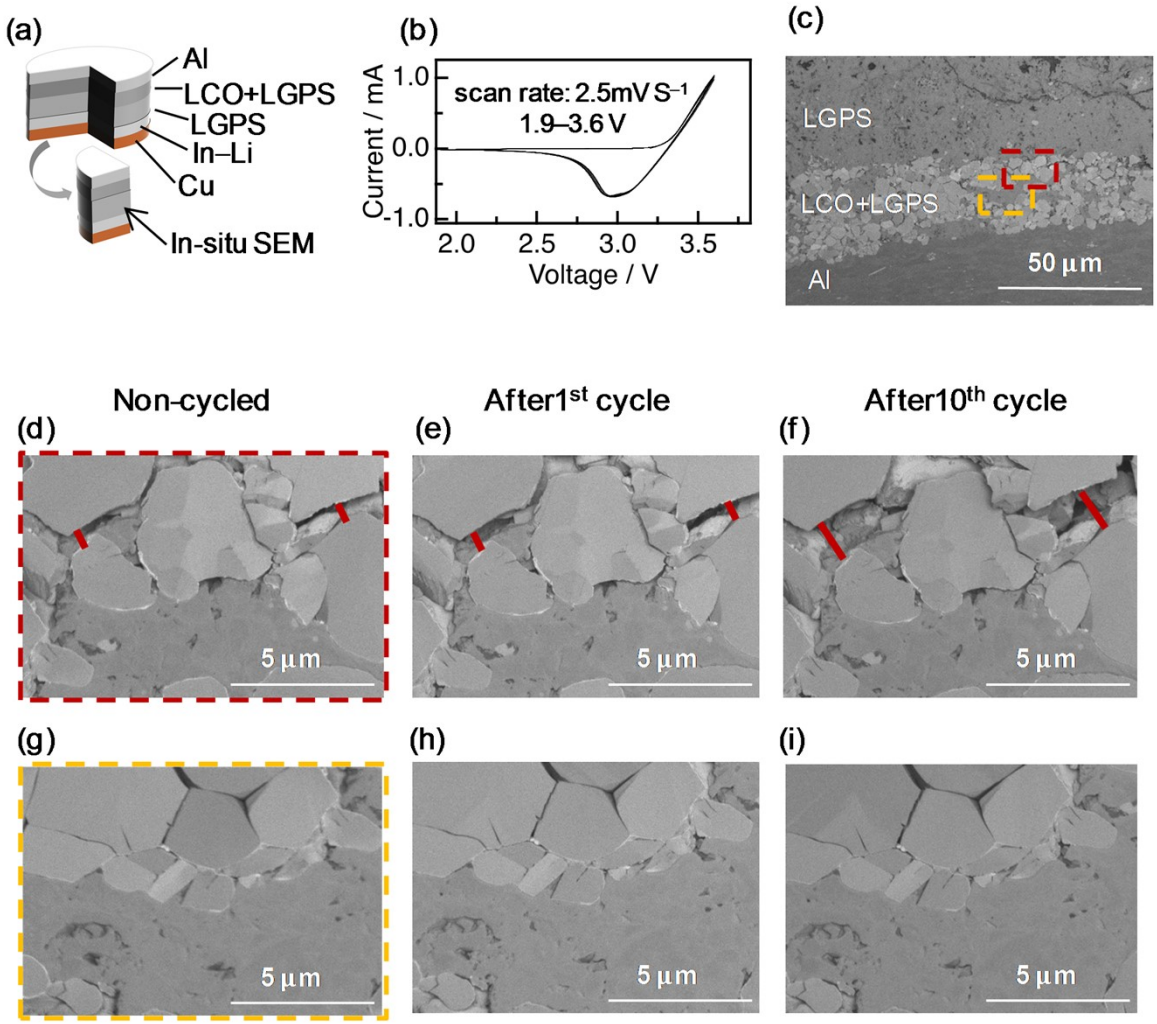

Fig. S1 *In situ* FE-SEM observations of the composite cathode. (a) The cell layout and observation direction. (b) The cyclic voltammetry result with a scan rate of 2.5 mV s^{-1} over a voltage range of 1.9–3.6 V. (c) Cross-sectional images of cathode layers before cycles. (d)-(f) The amplified images of the red rectangle marked area in (c) before cycles and after 1st and 10th cycles, where the contact decrease is significant and pointed out by red lines. (g)-(i) The amplified images of the yellow rectangle marked area in (c) before cycles and after 1st and 10th cycles, where the contact decrease is not detectable. These observations indicate that the decrease in contacts between particles in the composite cathode progressed continuously and in an uneven manner upon increasing the number of charge–discharge cycles.

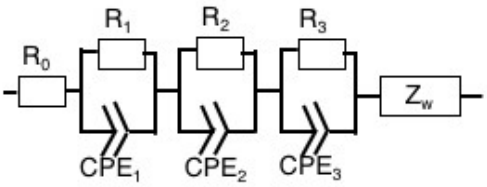

Fig. S2 Equivalent circuit for fitting of the EIS in this study.[1, 2] R_0 is the solid electrolyte resistance, $R_1|CPE_1$ combined with $R_2|CPE_2$, and $R_3|CPE_3$ represent the contributions mainly from the cathode and the anode sides, respectively. R is the resistor component and the constant phase element (CPE) is the capacitor component. Z_w is the Warburg diffusion component. The fitting parameters of the equivalent model for the cells are listed in **Table S1** for cells shown in Figs. 3 and 5 in main text. The equations used to connect the mathematical parameters of CPE and the corresponding capacitance value are described elsewhere.[1]

Table S1 Fitting parameters for the cells employed in this work

Cell		R_0 / Ω	R_1 / Ω	C_1 / F	R_2 / Ω	C_2 / F	R_3 /Ω	C_3 / F
Fig. 2	50th	14	107	2.8×10^{-9}	588	2.4×10^{-8}	75	1.8×10^{-3}
	re-pressed	13	105	1.8×10^{-9}	132	1.6×10^{-7}	102	3.0×10^{-4}
Fig. 4	1st	11	39	2.4×10^{-7}	6	2.5×10^{-7}	49	2.1×10^{-3}
	cycled	11	85	4.1×10^{-9}	566	4.8×10^{-8}	169	2.4×10^{-4}
	heated	10	26	4.8×10^{-6}	167	1.6×10^{-6}	44	2.2×10^{-3}

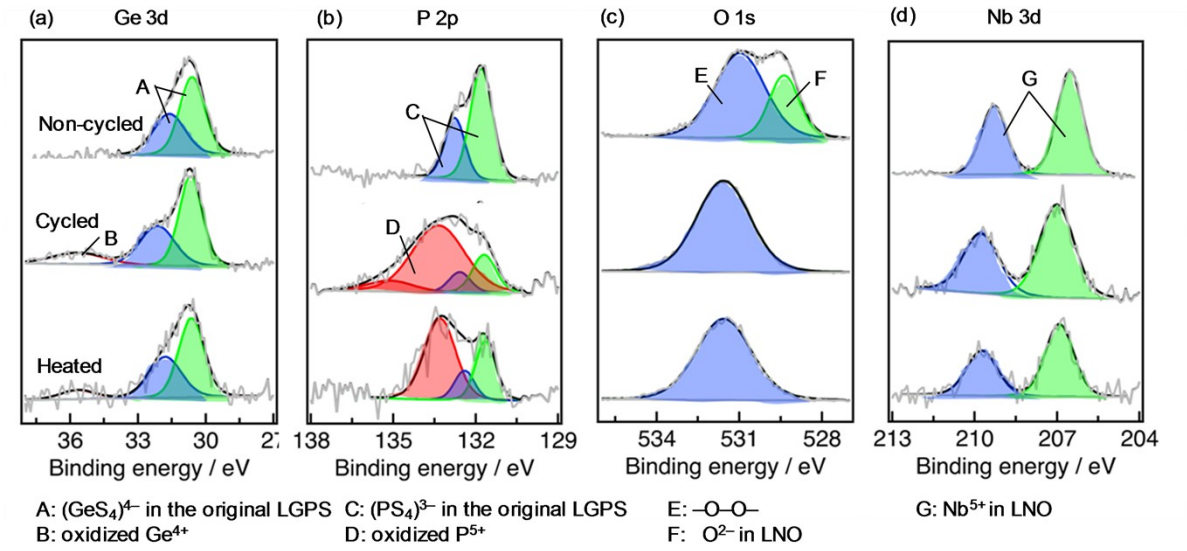

Fig. S3 High-resolution X-ray photoelectron spectra of the (a) Ge 3d, (b) P 2p, (c) O 1s, and (d) Nb 3d edges collected from the cathodes of the non-cycled normal cell (Non-cycled) and the cell after 100 cycles (Cycled), as well as the cell with a heated cathode after one cycle (Heated). Intensities are normalized for comparison. Fitting parameters are listed in **Table S2.**

Table S2 Fitting parameters for XPS in **Fig. 3** of the main text and **Fig. S3**

	Non-			Cycled			Heated		
	Pos. /eV	FWHM	At. %	Pos.	FWHM	At. %	Pos.	FWHM	At. %
S	160.8	1.2	67	160.9	1.2	26	160.8	1.3	38
	162.0	1.2	33	162.1	1.1	13	161.9	1.2	19
	–	–	–	162.8	2.6	27	162.8	2.1	9
	–	–	–	166.7	1.1	7	166.6	1.2	10
	–	–	–	169.0	2.3	27	168.7	2.4	24
P	131.	1.0	6	131.6	1.0	17	131.7	0.9	28
	132.8	0.9	33	132.4	0.9	8	132.4	0.9	14
	–	–	–	133.2	2.3	66	133.3	1.3	59
Ge	30.7	1.3	60	30.7	1.2	51	30.8	1.3	55
	31.8	1.7	40	31.9	1.8	34	31.8	1.7	36
	–	–	–	35.3	2.7	15	35.5	1.9	9
O	529.4	1.3	30	531.6	2.3	100	531.6	2.4	100
	531.0	2.2	70	–	–	–	–	–	–
Nb	206.8	1.1	60	207.1	1.5	60	206.9	1.2	60
	209.6	1.1	40	209.9	1.5	40	209.7	1.3	40

XPS analysis was performed to compare the chemical changes in the cells. In comparison with the non-cycled cathode, the other two cathodes exhibited spectral changes, indicating that an interfacial chemical reaction had occurred. The XPS changes in this work are consistent with previously reported results.[2, 3] The similarity of the S 2p spectra of the 100-times cycled cell and the heated cell is discussed in the main text and is shown in **Fig. 3**. It was also found that the Ge 3d, P 2p, O 1s, and Nb 3d spectra also exhibited similarities. These spectral changes indicate the generation of interphases (*e.g.,* sulfur, metal sulfates, germanium oxide, metaphosphate, and/or P_4O_{10}.) in the interfacial region.

In addition, the changes observed between the O 1s spectra of the non-cycled and the cycled samples coincide with the changes of the EELS results presented in **Fig. S6**. Analysis of the changes in the O 1s edge observed by XPS support the interpretation of the EELS results on the O_K edge.

The O 1s signal here is mainly derived from the LNO layer due to the probing depth of the XPS method (typically 4–5 nm). In the non-cycled cathode, the O 1s spectrum was deconvoluted into two elements, namely the metal oxide with a BE of 529.5 eV (peak-F) and the peroxide with a BE of 531.5 eV (peak-E). After 100 cycles, the oxygen became oxidized and reached a state with a BE of 532 eV, which was ascribed to the BE of sulfate.[4]

Among the obtained XPS results, the S 2p edge profiles showed the most significant and distinguishable changes. Considering the high sensitivity of the S 2p signal to chemical degradation, these spectral changes can be used as an indicator of the degree to which the interface reaction had taken place. Thus, the ratio between the spectral peak areas for the oxidized region and the original region were compared. It was found that the ratio was similar for the cycled cell (33.5%) and the heated cell (34.1%), thereby implying that the chemical reaction in the cycled cell was well simulated in the heated cell.

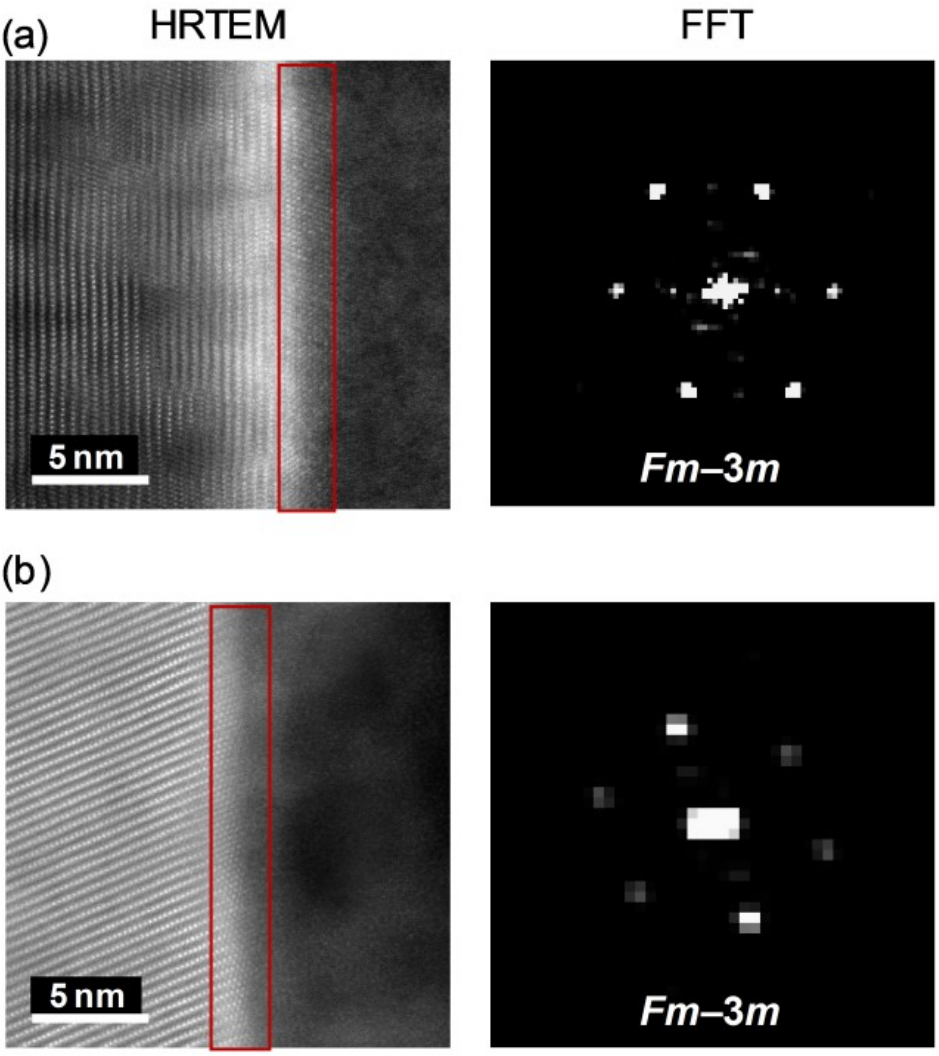

Fig. S4 High-resolution TEM (HRTEM) images of the LCO/LNO interface region and the corresponding fast Fourier transform (FFT) patterns of the cells (a) before charge–discharge cycling, and (b) after 100 cycles. HRTEM was performed to investigate the crystal structure at the LCO/LNO/LGPS interface region before and after cycling. HRTEM and FFT images indicated that no structural changes took place in the bulk-LCO, the LNO/LCO interface, or the bulk-LNO. Details regarding the FFT simulation patterns are presented in **Fig. S5**.

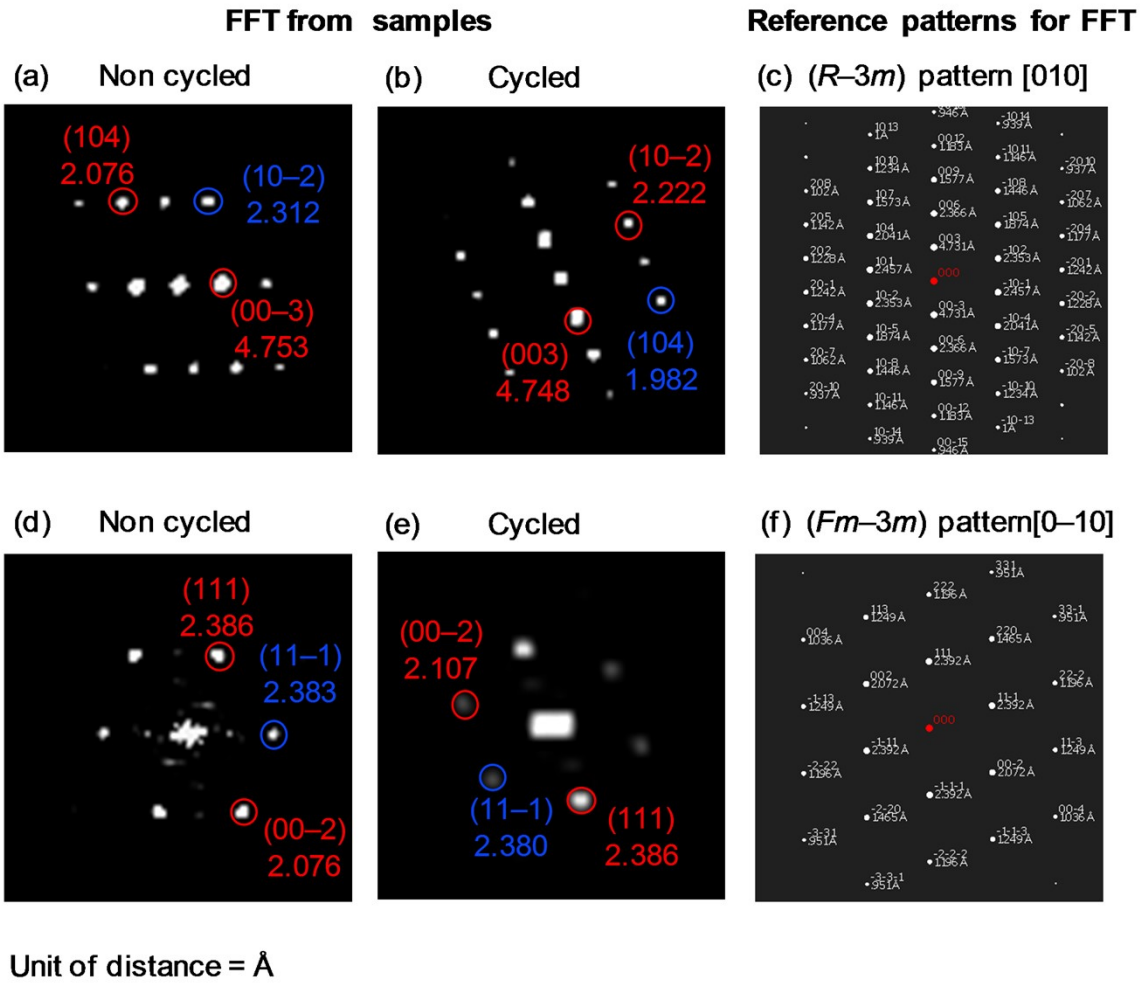

Fig. S5 FFT simulations for the HRTEM images shown in Fig. 6 in the main text. FFT analysis was performed for the areas at distances of (a–c) 10 nm and (d–f) 3 nm from the interface; (a and d) non-cycled cells, (b and e) the cycled cell, and (c and f) simulation. The FFT patterns were calibrated using Digital Micrograph software (Gatan).

For the area at a distance of 10 nm from the LCO surface, patterns for (a) the non-cycled and (b) the cycled cells matched with a layered structure (space group: $R\bar{3}m$), which is ascribed to the bulk-LCO. In addition, FFT analysis of the selected area electron diffraction (SAED) data for the bulk areas for both the non-cycled and the cycled LCO also indicated the presence of a layered structure in the bulk area (data are not presented here). For the area at a distance of 3 nm from the LCO surface, shown in the red rectangle of **Fig. S4**, both patterns match the NaCl-type structure (space group: $Fm\bar{3}m$), which is ascribed to the LCO surface.[5] These observations indicate that the LCO structure was retained in the bulk and on the surface after 100 cycles.

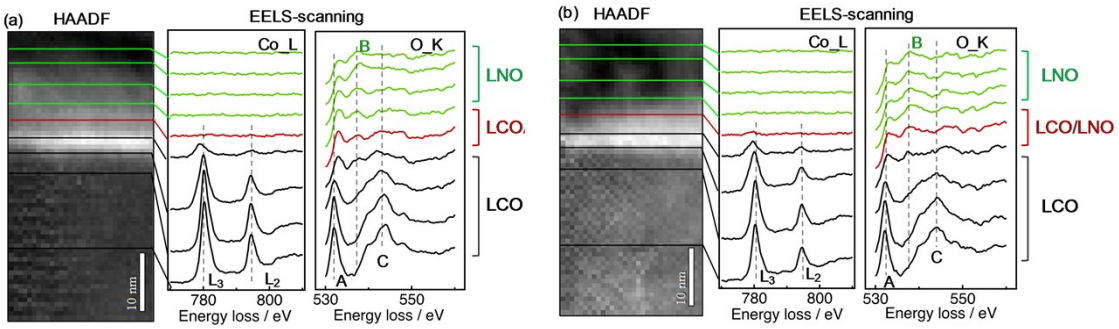

Fig. S6 High-angle annular dark-field (HAADF) images and the corresponding EELS line scans for the Co_L and O_K edges across the interface for (a) the non-cycled cell, and (b) the cycled cell. Each EELS spectrum was collected from the respective area shown in the HAADF image.

The spectra shown in green, red, and black were collected from the LNO layer, the LNO/LCO interface, and the LCO layer, respectively. In both cells, upon moving from the bulk to the surface, the peaks corresponding to Co_L (L_2 and L_3) shifted to the lower energy loss direction (i.e., to the left in each panel). This observation indicates that the Co valence decreased from the bulk to the surface.[6, 7] In both samples, above the LCO/LNO interface (i.e., in the LNO layer), which is marked by a red line in the HAADF panels, almost no Co signal was detected, indicating that very little Co diffusion into the LNO layer took place. No difference was detected in the chemical state of Co before and after cycling.

In the O_K edge, three peaks were observed in the spectra for both the non-cycled cell and the cycled cell. Peak-A for the O_K edge, observed at ~532 eV in the LCO side, was attributed to the O 2p–Co 3d (in the LCO layer) and the O 2p–Nb 4d (in the LNO layer) hybridised orbitals.[8] In addition, peak-B, which was observed at ~538 eV in the LNO side, was attributed to the e_g component of the split Nb 4d–O 2p orbital, while peak-C (~544 eV in the LCO side) was ascribed to multiple scattering by the oxygen neighbours present in the cluster, or the O 2p–Co 4sp hybridised orbital.[9, 10] Upon comparison of the two cells, it was apparent that peak-A and peak-C showed similar profile changes from the LCO bulk to the LCO/LNO surface, indicating the cyclic stability of the LCO bulk. In the LNO layers of both cells, the observation of peak-A and peak-B indicates that the amorphous LNO layer contains Nb–O covalent bonds and short-range clusters. Since the ratio of peak-B to peak-A represents the change in the ratio of unoccupied orbit e_g/t_{2g} in the neighbouring Nb ions, this ratio can be used to indicate a change in the local environment of oxygen, such as the bond length or oxygen vacancy formation.[11, 12] In the non-cycled cell, the ratio of peak-B to peak-A varies from 0.39 to 1.68, while in the cycled cell, the ratio varies from 0.83 to 1.16, thereby indicating that the valence changes of Nb and O occurred in the LNO layer after cycling. This result is consistent with the O 1s XPS result (see **Fig. S3**), where the O 1s edge indicates an obvious change in chemical state from a mixture of the oxide and pre-oxide states to a sulfate oxide state.

References

1. Zhang, W.; Weber, D. A.; Weigand, H.; Arlt, T.; Manke, I.; Schröder, D.; Koerver, R.; Leichtweiss, T.; Hartmann, P.; Zeier, W. G., Interfacial processes and influence of composite cathode microstructure controlling the performance of all-solid-state lithium batteries. *ACS applied materials & interfaces* **2017,** *9* (21), 17835–17845.
2. Zhang, W.; Richter, F. H.; Culver, S. P.; Leichtweiss, T.; Lozano, J. G.; Dietrich, C.; Bruce, P. G.; Zeier, W. G.; Janek, J. r., Degradation mechanisms at the Li10GeP2S12/LiCoO2 cathode interface in an all-solid-state lithium-ion battery. *ACS applied materials & interfaces* **2018,** *10* (26), 22226–22236.
3. Gittleson, F. S.; El Gabaly, F., Non-faradaic Li+ migration and chemical coordination across solid-state battery interfaces. *Nano letters* **2017,** *17* (11), 6974-6982.
4. Chastain, J.; King Jr, R. C., Handbook of X-ray photoelectron spectroscopy. *Perkin-Elmer Corporation* **1992,** *40*, 221.
5. Geder, J.; Hoster, H. E.; Jossen, A.; Garche, J.; Denis, Y., Impact of active material surface area on thermal stability of LiCoO2 cathode. *Journal of Power Sources* **2014,** *257*, 286-292.
6. Okubo, M.; Kim, J.; Kudo, T.; Zhou, H.; Honma, I., Anisotropic surface effect on electronic structures and electrochemical properties of LiCoO2. *The Journal of Physical Chemistry C* **2009,** *113* (34), 15337–15342.
7. Pearson, D.; Ahn, C.; Fultz, B., White lines and d-electron occupancies for the 3d and 4d transition metals. *Physical Review B* **1993,** *47* (14), 8471.
8. De Groot, F.; Grioni, M.; Fuggle, J. C.; Ghijsen, J.; Sawatzky, G. A.; Petersen, H., Oxygen 1s x-ray-absorption edges of transition-metal oxides. *Physical Review B* **1989,** *40* (8), 5715.
9. Graetz, J.; Hightower, A.; Ahn, C.; Yazami, R.; Rez, P.; Fultz, B., Electronic structure of chemically-delithiated LiCoO2 studied by electron energy-loss spectrometry. *The Journal of Physical Chemistry B* **2002,** *106* (6), 1286–1289.
10. Kurata, H.; Lefevre, E.; Colliex, C.; Brydson, R., Electron-energy-loss near-edge structures in the oxygen K-edge spectra of transition-metal oxides. *Physical Review B* **1993,** *47* (20), 13763.
11. Chen, C.; Yin, D.; Inoue, K.; Lichtenberg, F.; Ma, X.; Ikuhara, Y.; Bednorz, J. G., Atomic-Scale Origin of the Quasi-One-Dimensional Metallic Conductivity in Strontium Niobates with Perovskite-Related Layered Structures. *ACS Nano* **2017,** *11* (12), 12519–12525.
12. Carroll, K. J.; Qian, D.; Fell, C.; Calvin, S.; Veith, G. M.; Chi, M.; Baggetto, L.; Meng, Y. S., Probing the electrode/electrolyte interface in the lithium excess layered oxide Li1.2Ni0.2Mn0.6O2. *Physical Chemistry Chemical Physics* **2013,** *15* (26), 11128–11138.